OPEN ACCESS
IOP Publishing

Letters
Journal of Physics D: Applied Physics

J. Phys. D: Appl. Phys. **50** (2017) 42LT01 (7pp)
https://doi.org/10.1088/1361-6463/aa8ae4

Letter

Quantum well engineering in InGaN/GaN core-shell nanorod structures

C G Bryce[1], E D Le Boulbar[2], P-M Coulon[2], P R Edwards[1], I Gîrgel[2], D W E Allsopp[2], P A Shields[2] and R W Martin[1,3]

[1] Department of Physics, SUPA, University of Strathclyde, Glasgow, G4 0NG, United Kingdom
[2] Department of Electrical and Electronic Engineering, University of Bath, Bath, BA2 7AY, United Kingdom

E-mail: r.w.martin@strath.ac.uk

Received 11 August 2017, revised 5 September 2017
Accepted for publication 7 September 2017
Published 27 September 2017

Abstract

We report the ability to control relative InN incorporation in InGaN/GaN quantum wells (QWs) grown on the semi-polar and non-polar facets of a core-shell nanorod LED structure by varying the growth conditions. A study of the cathodoluminescence emitted from series of structures with different growth temperatures and pressures for the InGaN QW layer revealed that increasing the growth pressure had the effect of increasing InN incorporation on the semi-polar facets, while increasing the growth temperature improves the uniformity of light emission from the QWs on the non-polar facets.

Keywords: nanostructure, InGaN, cathodoluminescence, LED, GaN, nanorod

(Some figures may appear in colour only in the online journal)

1. Introduction

The advantages of fabricating InGaN/GaN QW-based LEDs in a core-shell structure compared to planar growth have been well discussed [1–3]. Attention is often drawn to advantages such as the increased surface area of emission, reduced influence of the Auger effect due to the reduced carrier density afforded by the greater QW coverage, and access to low defect m-plane surfaces—a benefit of the nanorods' reduced footprint on the substrate [4]. Carrier recombination occurring within the QW at these non-polar sidewalls is less subject to the crystal's intrinsic electric field, simultaneously reducing the quantum-confined Stark effect (QCSE) and increasing electron-hole wavefunction overlap in this geometry compared to QWs on polar or semi-polar surfaces. These factors make it particularly desirable to be able to control the homogeneity of InN content throughout the QW shell layer. It is known that when growing InGaN by metal organic vapour phase epitaxy (MOVPE), the InN content can be controlled by means of the temperature in the reactor. A higher growth temperature reduces the InN fraction in the resulting layer, causing its bandgap to increase [5, 6]. It is also possible to control InN incorporation by altering the pressure within the reactor: a higher growth pressure increases the frequency of the In-containing species colliding with the growth surface, and inhibits In desorption. Both of these effects improve incorporation of InN [7]. The issue, then, is twofold: firstly, is it possible to incorporate enough InN that the QW emission becomes tunable by varying growth conditions; and secondly, can this incorporation be done uniformly down the full length of a nanorod sidewall, to optimise emission from the material? These factors are considered here, through a study of InGaN/GaN core-shell nanorods grown at varying temperatures and pressures.

[3] Author to whom any correspondence should be addressed.

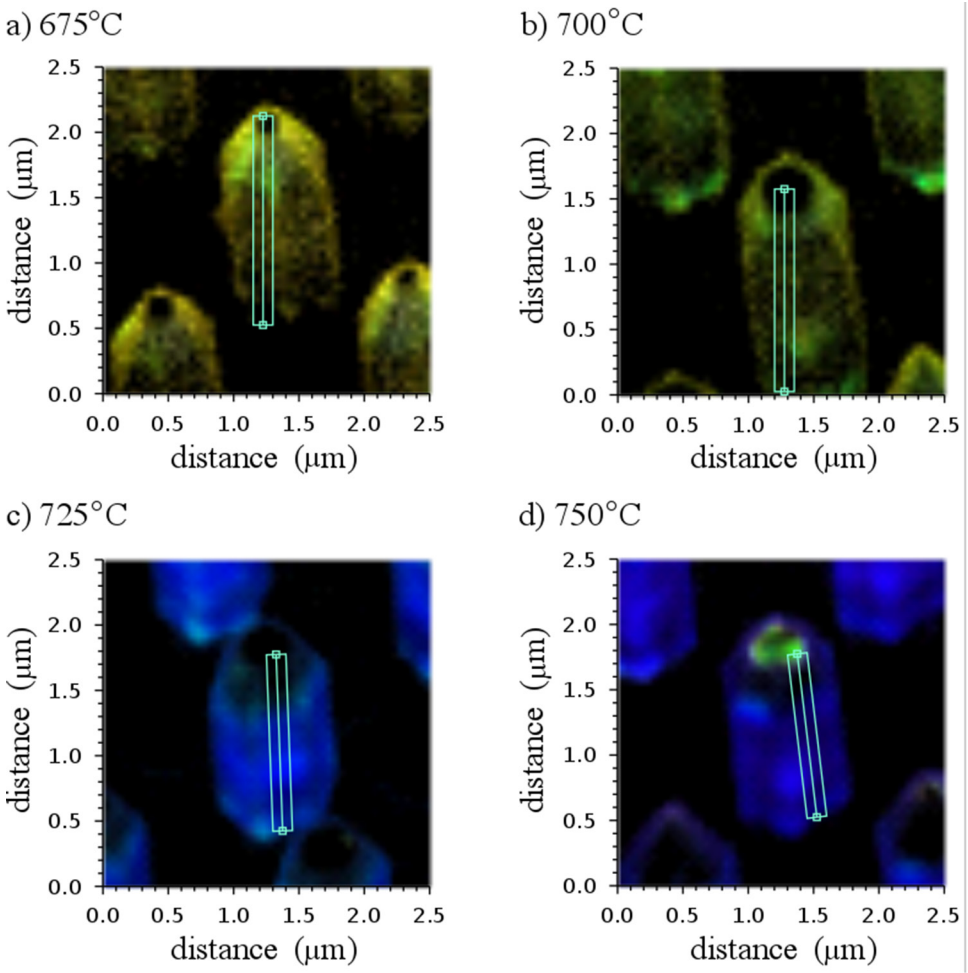

Figure 1. 'Real' colour hyperspectral CL maps of InGaN/GaN core-shell nanorods where the growth temperature of the InGaN layer has been varied between 675 °C (a) to 750 °C (d) in steps of 25 °C. It should be noted that for true real colour the data should encompass the entire visible spectrum, whereas here only the 1.82 eV to 3.52 eV range has been measured.

2. Methods

The top-down/bottom-up hybrid approach to creating a core-shell nanorod is to first etch a scaffold of 'core' rods in a GaN epilayer and subsequently grow new material in a 'shell' surrounding the rods. In this work this is achieved by using nanoimprint lithography with a Ni coating over a GaN-on-silicon substrate to define an array of Ni nanodots which then serve as a mask before the sample is etched in an inductively coupled plasma to leave an array of nanorods approximately 1 μm tall standing under the areas of the sample covered by the Ni mask [8]. For long etch times (required to obtain high aspect ratio rods), this often leads to the sidewalls of the rods being uneven. As this would significantly affect the distribution of any QW material subsequently deposited, there is a second GaN growth at this point, to recover smooth facets [9]. This occurs at 975 °C for eight minutes: four minutes at 200 mbar and four at 100 mbar. After facet recovery, the InGaN QW is grown. Results on two series of samples are presented in this work. For the first, looking at the effect of growth temperature, the QWs were grown for six minutes at temperatures varying between 675 °C and 750 °C under a pressure of 150 mbar. The second studied the effect of growth pressure, which was varied between 150 mbar and 450 mbar at a temperature of 725 °C, also for six minutes. The QW layer thickness is estimated to be approximately 5 nm based on a growth rate of 0.75 nm min^{-1} at 700 °C observed in similar samples. Growth concludes with a 2.5 nm capping layer of GaN grown at 900 °C under a pressure of 100 mbar for 5 min, to complete the core-shell structure.

The optical and topographical properties of the samples were investigated using an FEI Quanta 250 FEG scanning electron microscope, modified to capture room temperature cathodoluminescence (CL) spectra as well as a range of other information resulting from electron beam excitation [10]. As the electron beam is scanned across the sample, impact ionisation generates electron-hole pairs which can recombine to produce the CL signal. This signal is collected by a reflecting objective telescopic mirror set-up to reflect towards a crossed Czerny-Turner spectrometer (Oriel MS125), which diffracts it towards a 1600-element electron multiplying charge-coupled device (EMCCD) [11]. For each of the samples investigated in this report, a 5 kV accelerating voltage was used to collect data in 40 nm steps across the sample, and a 600 lines mm^{-1} grating blazed at 400 nm diffracted the light collected via a 50 μm entrance slit. The exit slits are defined by the width of the pixel columns of the detector itself (16 μm) which operates in full vertical binning mode. The EMCCD was set to use

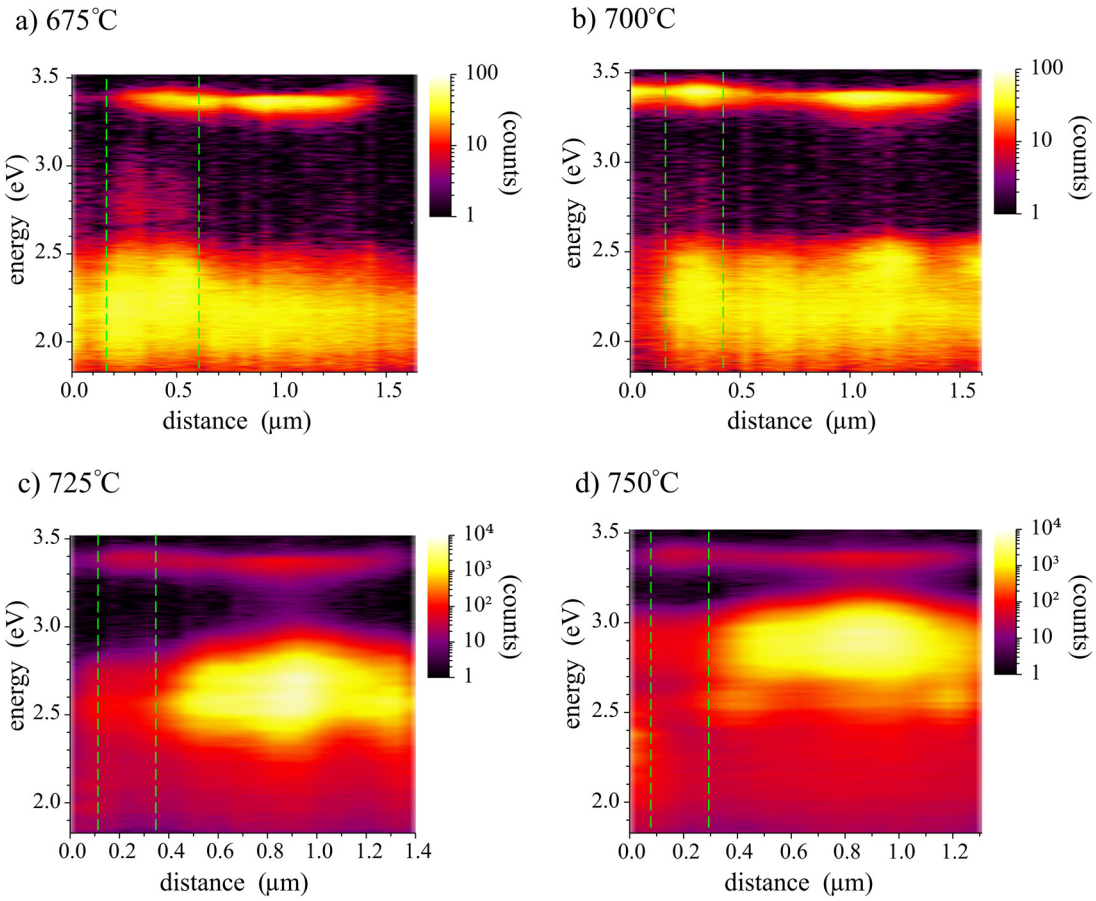

Figure 2. Linespectra from tip to base of individual InGaN/GaN nanorods where the QW layer has been grown at temperatures between 675 °C (a) and 750 °C (d), showing variation in emission intensity and energy with position. Dotted lines indicate crystal facet boundaries.

2× horizontal binning (to give an effective 800 channels), a vertical read-out time of 9.75 μs, a horizontal read-out rate of 1 MHz, and the electron multiplying capability was used. These settings were chosen to optimise the signal-to-noise ratio. Unless otherwise stated, a beam current of (2.48 ± 0.50) nA was used for 100 ms of acquisition time. We estimate the excitation electrons to have lost 90% of their energy approximately 110 nm into the sample, based on CASINO software using Monte Carlo simulations to emulate our samples under a 5 kV electron beam incident at 45° as in our set up.

3. Results and discussion

Room temperature hyperspectral CL data were obtained from both sets of samples and analysed using custom written software [12]. The dataset from the growth temperature dependant series is first presented in more detail as a working example of our analysis, followed by the pressure dependant series dataset.

3.1. Growth temperature variation

Figure 1 shows 50 × 50 pixel hyperspectral CL data rendered in colours generated from the emission spectra measured at each 50 nm step of the maps. For each sample a stack of averaged spectra, moving from the tip to the base, was constructed using three-pixel wide linescans, which are highlighted in figure 1. The resulting CL intensity profiles are shown in figure 2. Specific regions on the nanorods were selected using a cursor three pixels in diameter, such that about seven spectra could be averaged to give, for example, the typical spectrum from a sloping semi-polar facet seen in figure 3(c). This was performed for all nanorods where the facet in question was available so as to ensure a representative dataset. These spectra were fitted with Gaussian functions in order to extract the emission energy of the QW peak, which exists between the defect ('yellow'-) band centred at about 2.2 eV and the GaN band edge centred at about 3.4 eV. A representative spectrum for the yellow-band was subtracted from the datasets such that peaks attributable to defect luminescence would not influence analysis. This information is then used to investigate the energy and intensity of the QW emission with respect to increasing the growth temperature of the InGaN layer, presented here as figures 3(a) and (b).

We focus our analysis on variations seen in CL intensity and peak energy as a function of growth temperature, as well as the consistency of both of these within a single region on a nanorod, referred to as *uniformity* of the emission. Firstly, emission from the non-polar sidewalls shows increases in peak energy and uniformity with increasing growth temperature. This is because the likelihood of In atoms to desorb from the surface increases at higher growth temperatures, resulting in a InGaN layer with lower InN content. As such increasing

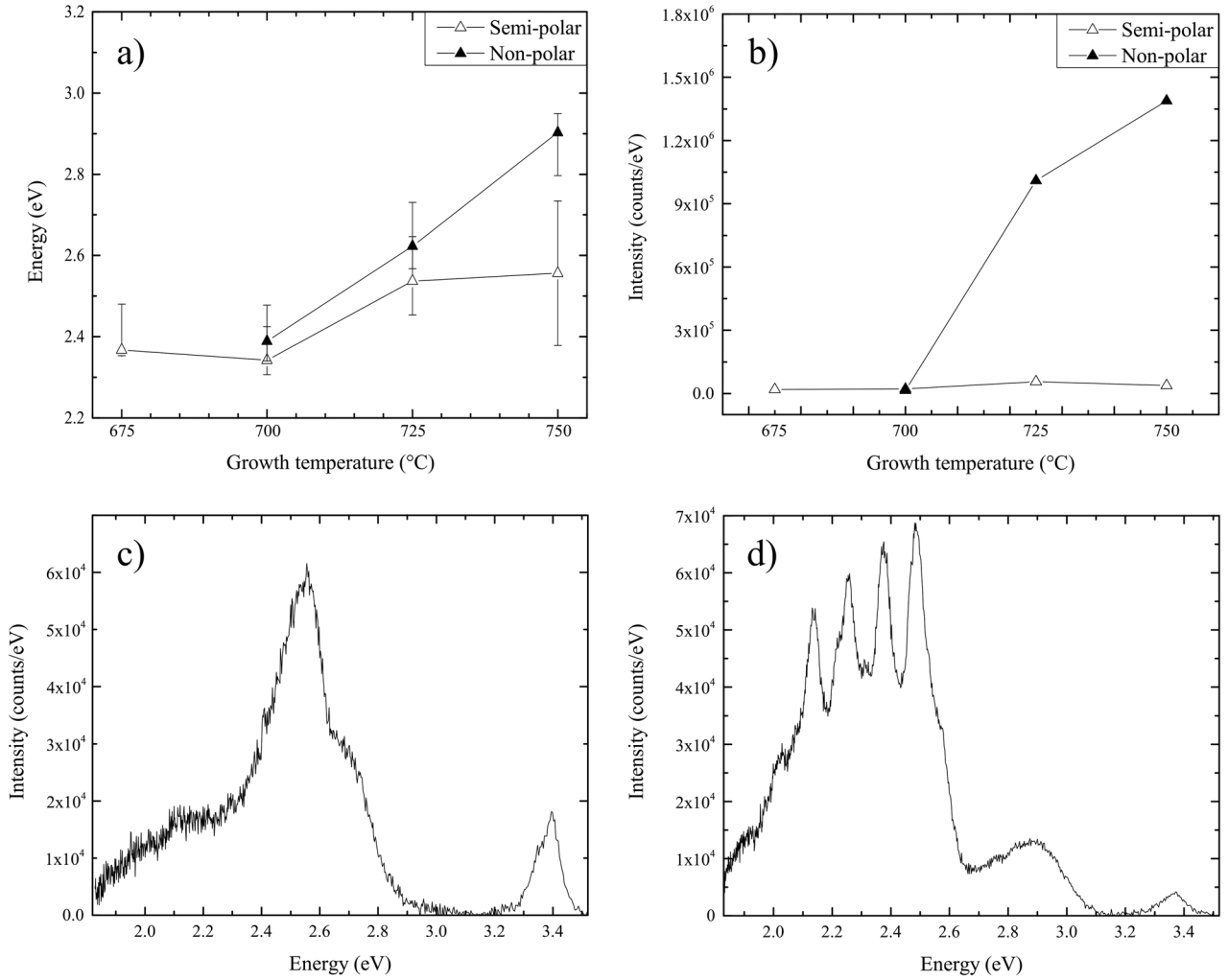

Figure 3. Variation in CL peak energy (a) and intensity (b) from different facets on InGaN/GaN core-shell nanorods with respect to varying QW layer growth temperature. Plot (c) shows the average of 50 spectra seen from a semi-polar facet, while plot (d) shows the average of nine spectra extracted from c-plane of the nanorod mapped in figure 1(d).

the growth temperature has the effect of increasing the energy bandgap, so a blueshift in the emission is to be expected.

Secondly, increasing growth temperature leads to a dramatic increase in the intensity of emission from the non-polar facets relative to the semi-polar facets, as seen in figure 3(b). We attribute this primarily to the different rates of change of InN incorporation with temperature between the two types of plane. As the growth temperature increases, the InN content drops 2–3 times faster on the non-polar planes compared to the $\{1\,0\,\bar{1}\,1\}$ semi-polar planes [13, 14]. This more rapid drop in InN content causes a faster improvement in material quality for the non-polar planes and produces the rapid increase in intensity relative to the semi-polar planes. Reducing InN content would be expected to reduce the negative impact of the QCSE in the semi-polar planes and thus increase the emission intensity, but the lower rate of change of the InN content has reduced the impact of this change. Other effects may also contribute, including the observed reduction in quantum well thickness for semi-polar [13] and the fact that the changed InN incorporation may make the growth conditions less optimised for one of the faces (in this case the semi-polar).

Thirdly, a broadening of the spectral peaks occurs at the intersections between faces, where a reduction in the emission intensity can also be noted from figure 1. The broadening is accounted for if the edges of the rods are areas where the crystal has relaxed, for if so, they would be favourable for InN incorporation, creating localised regions with a lower bandgap and hence lowering emission energy from such regions [15]. The reduction in intensity may be due to competition with emission from the middle of the non-polar planes, where the well-formed QW provides strong emission [13]. This region may also be benefitting from enhancement due to CL coupling to optical modes within the nanorod.

The final point to note from this data is that figures 1 and 2(d) show emission highly localised to the polar c-planes at the tips of some rods, comprised of multiple sharp peaks 110 meV apart, as seen in figure 3(d). The even spacing of these peaks suggests they arise from optical modes, with the nanorod acting as a Fabry–Perot cavity. The mode spacing corresponds to a cavity approximately 2 μm in length, which could either be due to a 'vertical' cavity along the length of the rod or due to the filtering of longer wavelength emission

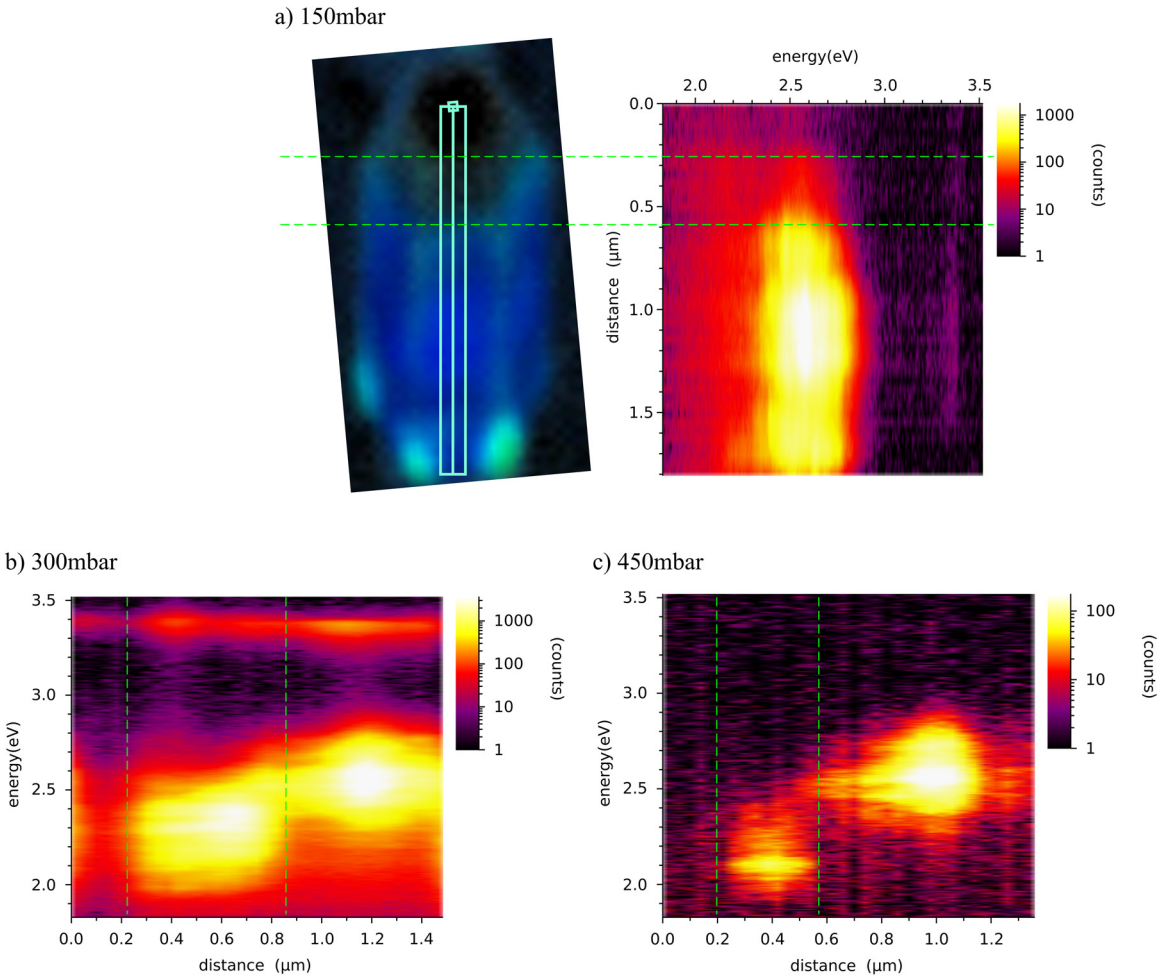

Figure 4. Linespectra from tip to base of individual InGaN/GaN nanorods where the QW layer has been grown at pressures between 150 mbar (a) and 450 mbar (c). Variation in emission intensity and energy from the different facets can be seen. Dotted lines indicate crystal facet boundaries.

from the tip by whispering gallery modes in the bulk of the rod [16].

3.2. Growth pressure variation

A similar process was followed with the CL data obtained from samples where the growth pressure of the InGaN layer has been varied from 150 mbar to 450 mbar in 150 mbar steps. Both series contain a sample grown at 725 °C and 150 mbar (see figures 1(c) and 5(a)), providing a link between the two. Figures 4–6 summarise the results, using the same methodology as for the first series of nanorods. Unlike the temperature dependant series, direct comparisons of peak intensity between these samples are avoided as these were not measured all in the same experimental run, however it is both valid and informative to consider variations between different spectral regions within a given map, as seen in figure 4.

Figure 5(d) provides an example of the fitting used to analyse the data in these maps. A Gaussian curve is fit across the spectral region of interest, and the adjusted map is then interrogated at multiple locations to extract the behaviour of the CL peak at, in this case, the non-polar planes of rods grown at a pressure of 300 mbar.

As in the series where the growth temperature of the InGaN layer was varied, little to no CL is seen from the tips of the rods, and that from edges of the rods tends to be spectrally broader. This suggests that this is not related to the growth conditions but is a feature of the rods. The observed broadening of the spectra at edges on the rods towards lower energies is indicative of a larger InN fraction and relaxation of strain [17, 18]. The lack of QW emission from the tips of the rods is likely due to a combination of the QCSE limiting radiative recombination from the available c-planes, and a higher number of structural defects preventing luminescence.

Unlike the previous series, figure 6 shows the energy of the emission coming from the non-polar m-planes does not shift with the changing growth condition but the emission from the semi-polar planes does redshift by increasing the InGaN growth pressure. We suggest that this is due to the higher pressure in the chamber suppressing desorption and therefore leading to a relatively higher InN fraction.

Comparing results from both series reveals significantly different behaviours for the semi-polar and non-polar planes of the nanorods, suggesting it is possible to control QW incorporation by varying growth conditions. We note the fast increase in emission intensity from the non-polar

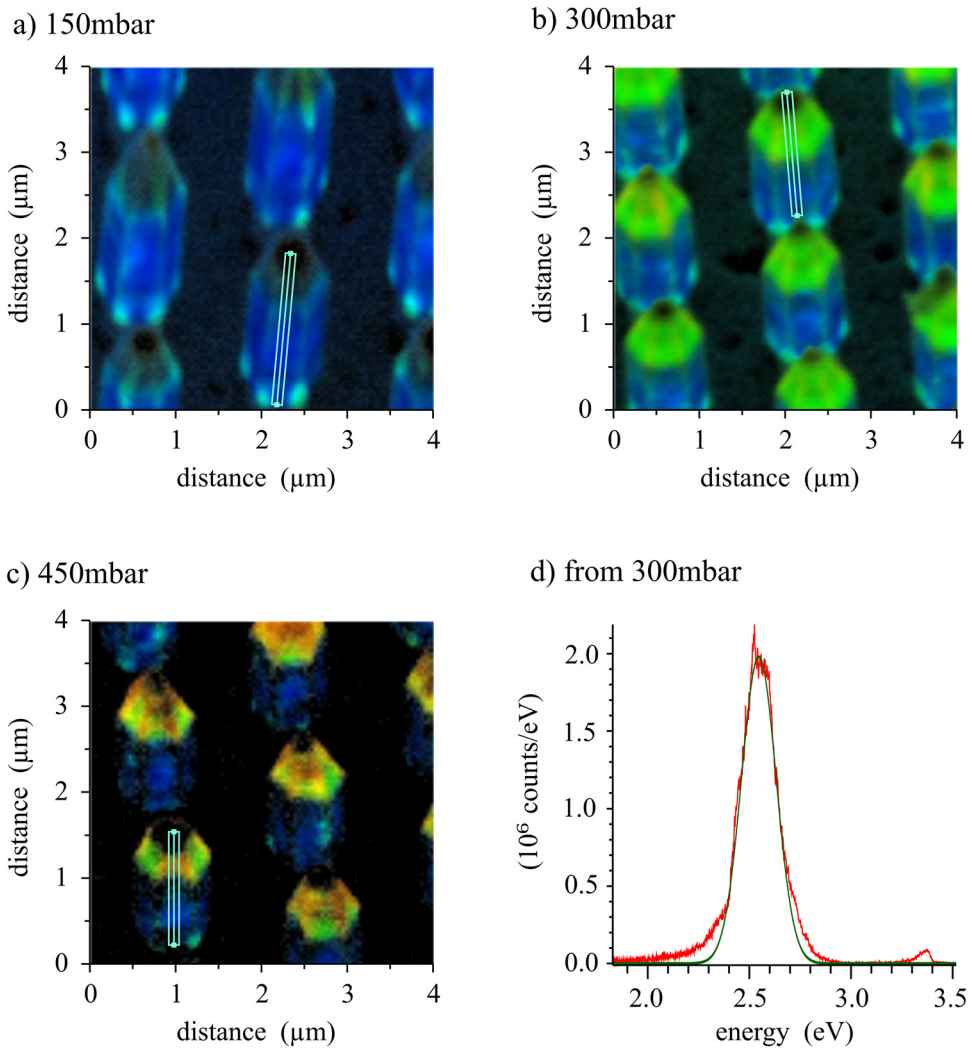

Figure 5. 'Real' colour hyperspectral CL maps of InGaN/GaN core-shell nanorods where the growth pressure of the InGaN layer has been varied from 150 mbar (a) to 450 mbar (c) in steps of 150 mbar. An example of the fitting used in analysing the maps is shown in (d), where the measured spectrum is extracted from the middle of an m-plane visible in (b) and the fit is a Gaussian.

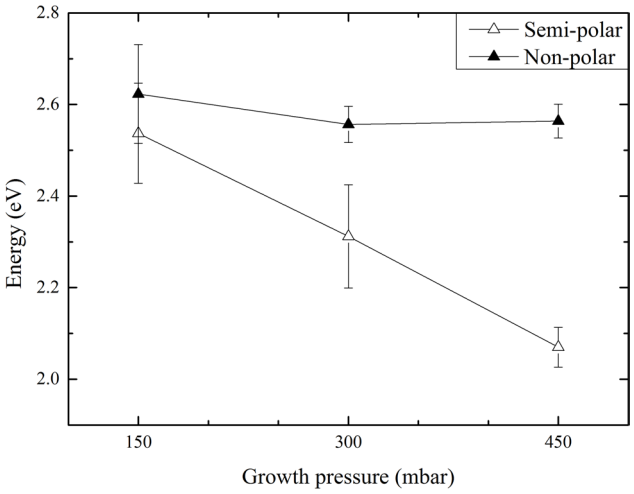

Figure 6. Behaviour of InGaN/GaN core-shell nanorod emission from different facets with respect to varying growth pressures.

planes with increased growth temperature, and a lack of energy shift in emission from these planes with increasing growth pressure.

4. Conclusions

In summary, the optical properties of InGaN/GaN core-shell nanorods where the QW layers were grown at different temperatures and pressures have been characterised by means of a CL study. It was found that increasing the growth temperature during inclusion of the InGaN QW layer while maintaining a fixed growth pressure affects the incorporation of InN into the non-polar planes on the nanorods, improving the emission intensity and its uniformity down the length of the nanorod. By fixing the growth temperature and increasing the growth pressure however, InN incorporation on the semi-polar planes is enhanced, as indicated by a redshift in emission from these planes.

Acknowledgments

The authors would like to thank the EPSRC for funding this work through the project 'Manufacturing of nano-engineered III-nitride semiconductors' (EP/M015181/1). Datasets are accessible at https://doi.org/10.15129/e30bcec8-3f54-4a2b-9dd9-893e3651dfb7.

ORCID iDs

C G Bryce https://orcid.org/0000-0003-4577-3472
P R Edwards https://orcid.org/0000-0001-7671-7698
R W Martin https://orcid.org/0000-0002-6119-764X

References

[1] Yeh T W, Lin Y T, Stewart L S, Dapkus P D, Sarkissian R, O'Brien J D, Ahn B and Nutt S R 2012 *Nano Lett.* **12** 3257–62
[2] Mandl M *et al* 2013 *Phys. Status Solidi* **7** 800–14
[3] Zhao S, Nguyen H P T, Kibria M G and Mi Z 2015 *Prog. Quantum Electron.* **44** 14–68
[4] Hersee S D, Rishinaramangalam A K, Fairchild M N, Zhang L and Varangis P 2011 *J. Mater. Res.* **26** 2293–8
[5] Zhao Y *et al* 2012 *Appl. Phys. Lett.* **100** 201108
[6] Martin R W, Edwards P R, Pecharroman-Gallego R, Liu C, Deatcher C J, Watson I M and O'Donnell K P 2002 *J. Phys. D: Appl. Phys.* **35** 604–8
[7] Karpov S Y, Talalaev R A, Evstratov I Y and Makarov Yu N 2002 *Phys. Status Solidi* a **192** 417–23
[8] Lewins C J, Le Boulbar E D, Lis S M, Edwards P R, Martin R W, Shields P A and Allsopp D W E 2014 *J. Appl. Phys.* **116** 044305
[9] Le Boulbar E D, Gîrgel I, Lewins C J, Edwards P R, Martin R W, Šatka A, Allsopp D W E and Shields P A 2013 *J. Appl. Phys.* **114** 094302
[10] Edwards P R, Lethy K J, Bruckbauer J, Liu C, Shields P A, Allsopp D, Wang T and Martin R W 2012 *Microsc. Microanal.* **18** 1212–9
[11] Bruckbauer J, Edwards P R, Wang T and Martin R W 2011 *Appl. Phys. Lett.* **98** 141908
[12] Edwards P R and Martin R W 2011 *Semicond. Sci. Technol.* **26** 064005
[13] Le Boulbar E D *et al* 2016 *Cryst. Growth Des.* **16** 1907–16
[14] Wernicke T, Schade L, Netzel C, Rass J, Hoffmann V, Ploch S, Knauer A, Weyers M, Schwarz U and Kneissl M 2012 *Semicond. Sci. Technol.* **27** 024014
[15] Griffiths J T *et al* 2017 *Appl. Phys. Lett.* **110** 172105
[16] Kusch G, Conroy M, Li H, Edwards P R, Zhao C, Ooi B S, Pugh J, Cryan M J, Parbrook P J and Martin R W in preparation
[17] Zhuang Y D, Bruckbauer J, Shields P A, Edwards P R, Martin R W and Allsopp D W E 2014 *J. Appl. Phys.* **116** 174305
[18] Lu P F, Sun C, Cao H W, Ye H, Zhong X X, Yu Z Y, Han L H and Wang S M 2014 *Solid State Commun.* **178** 1–6